

The Innovations Approach to Single Frame Multichannel Blind Image Deconvolution

UDK xxx.xxx.xx

IFAC x.x;x.x.x (filled by editors)

Paper classification (filled by editors)

The linear mixture model (LMM) has recently been used for multi-channel representation of a blurred image. This enables use of multivariate data analysis methods such as independent component analysis (ICA) to solve blind image deconvolution as an instantaneous blind source separation (BSS) requiring no *a priori* knowledge about the size and origin of the blurring kernel. However, there remains a serious weakness of this approach: statistical dependence between hidden variables in the LMM. The contribution of this paper is an application of the ICA algorithms to the innovations of the LMM to learn the unknown basis matrix. The hidden source image is recovered by applying pseudo-inverse of the learnt basis matrix to the original LMM. The success of this approach is due to the property of the innovations of being more independent and more non-Gaussian than original processes. Our good, consistent simulation and experimental results demonstrate viability of the proposed concept.

Key words: blind deconvolution, image restoration, independent component analysis, innovations, statistically dependent sources

Višekanalna slijeva dekonvolucija slike zasnovana na inovacijama. Linearni model miješanja (LMM) se u posljednje vrijeme koristi i za višekanalnu reprezentaciju zamućene slike. Na taj se način multivarijantne metode analize podataka, poput analize nezavisnih komponenata (ICA), mogu iskoristiti i za rješavanje slijeve dekonvolucije slike bezmemorijskom slijepom separacijom izvora (BSS), a koja ne zahtjeva *a priori* znanje o veličini i podrijetlu jezgre zamućenja. Ipak, postoji velik nedostatak ovog pristupa: statistička zavisnost između skrivenih varijabli LMM-a. Doprinos ovog rada je primjena ICA algoritama na inovacijama LMM-a u postupku učenja nepoznate bazne matrice. Skriveno izvorne slike se restauriraju primjenom pseudo-inverza naučene bazne matrice na originalni LMM. Uspjeh predloženog pristupa se može zahvaliti svojstvu inovacija da su više nezavisne i više ne-gausovske od originalnog procesa. Dobri i konzistentni rezultati naših simulacija i eksperimenata demonstriraju upotrebljivost predloženog koncepta.

Ključne riječi: analiza nezavisnih komponenata, inovacije, restauracija slike, slijeva dekonvolucija, statistički zavisni izvori

1 INTRODUCTION

Blind deconvolution (BD) aims to reconstruct the original image from an observation degraded by spatially invariant blurring process and noise. Neglecting the noise term, the process is modeled as a convolution of a point spread function (PSF) $h(s,t)$ with an original source image $f(x,y)$ as:

$$g(x,y) = \sum_{s=-M}^M \sum_{t=-M}^M h(s,t) f(x-s, y-t) \quad (1)$$

where M denotes the PSF support size. If the PSF is known a number of algorithms are available to reconstruct original image $f(x,y)$ [1,2]. However, it is not always possible to measure or obtain information about a PSF, which is why BD algorithms are important [1]. In order to estimate the blurring kernel $h(s,t)$ a support size

has to be either given or estimated [1,2]. In general, estimation of the size of the blurring kernels is a non-trivial issue. Even in the most recent contributions it is assumed that estimation of the optimal value of the order of the blurring kernel is a serious issue [3]. Also, quite often *a priori* knowledge about the nature of the blurring process is assumed to be available [2] that is not always possible in practice. Multivariate data analysis methods, such as independent component analysis (ICA) [4], might be used to solve BD problem as an instantaneous BSS problem, where unknown blurring process would be absorbed into an unknown mixing or basis matrix. Thus, neither size of support nor origin of the blurring kernel would be required by the ICA approach to BD. However, multi-frame image required by the ICA LMM is not always available. Even if it is, it requires the blurring kernel to be non-stationary, which is true for blurring caused by atmospheric turbulence [5, 5a], but it is not

true for out-of-focus blur for example. Thus, an approach to single frame multichannel BD that requires minimum of *a priori* information about blurring process and original image would be of great interest. One such approach was proposed in [6]. It was based on a bank of 2-D Gabor filters [7] used due to their ability to realize multichannel filtering. A serious weakness of this approach to BD is that statistical independence assumption, upon which the ICA algorithms are built, among the hidden variables in the resulting LMM is not fulfilled. The reason is the special structure of the LMM that is obtained using Taylor series expansion of the source image, where the hidden variables are the source image and its spatial derivatives. That was realized in [8]. Therefore, non-negative matrix factorization (NMF) [9] has been employed in [10,11] to perform unsupervised decomposition of the LMM, hence BD, due to the fact that NMF algorithms are not sensitive to the statistical dependence among the hidden variables of the LMM. One potential problem with the NMF algorithms is that data non-negativity during formation of the LMM is not preserved. Fixing this problem influences sparseness of the LMM and consequently quality of the results. For this reason an approach to BD has been formulated in [12] combining ICA and multiscale subband decomposition, used to enhance statistical independence among the hidden variables of the LMM. The unknown mixing matrix is invariant with respect to the multiscale preprocessing transform and is estimated by applying ICA algorithms to the subband with statistically least dependent components. Hidden variables are recovered by applying a truncated SVD-based pseudoinverse of the learnt basis matrix to the data in original domain. The multiscale subband decomposition approach to enhance statistical independence is based on the assumption that wideband source signals are dependent, but there exist some narrow subbands where they are independent [13]. The main critique of the multiscale subband decomposition approach to BD introduced in [12] is its computational complexity if fine resolution in the subband decomposition process is necessary. This is due to the fact that 2D wavelet packets are used to implement the multiscale subband decomposition scheme. As an alternative to multiscale subband decomposition we propose in this paper an innovations representation of the LMM to enhance statistical independence among the hidden variables. Innovations present several nice properties important for the BD problem: (i) innovations are always more statistically independent and more non-Gaussian than original processes [14]; (ii) they have computationally efficient implementation in a form of the prediction-error filter estimated by means of the Levinson recursion [15]; (iii) they are data-adaptable. This means that the shape of the magnitude frequency response of the

prediction-error filter is adapted to the specific image, following profile of the statistical dependence among the hidden variables in the frequency domain. The rest of the paper is organized as follows. In section 2 we introduce the LMM of the degraded image and discuss its properties. Section 3 presents brief discussion related to the statistical properties of the source image in order to be amenable for BD by the proposed approach. Innovations representation is also described in section 3. Section 4 presents results of comparative performance analysis for simulated de-focused image, while section 5 presents results of the comparative performance analysis for experimental de-focused image. Conclusions are given in section 6.

2 INSTANTANEOUS LINEAR MIXTURE MODEL

The key insight in [6] was that original image $f(x-s, y-t)$ can be approximated by Taylor-series expansion around $f(x,y)$ giving:

$$\begin{aligned} f(x-s, y-t) = & \\ f(x, y) - sf_x(x, y) - tf_y(x, y) + & \quad (2) \\ s^2 f_{xx}(x, y) + t^2 f_{yy}(x, y) + stf_{xy}(x, y) - \dots & \end{aligned}$$

This enables to re-write (1) as:

$$\begin{aligned} g(x, y) = & \\ a_1 f(x, y) - a_2 f_x(x, y) - a_3 f_y(x, y) + & \quad (3) \\ a_4 f_{xx}(x, y) + a_5 f_{yy}(x, y) + a_6 f_{xy}(x, y) + \dots & \end{aligned}$$

where

$$\begin{aligned} a_1 = \sum_{s=-M}^M \sum_{t=-M}^M h(s, t), \quad a_2 = \sum_{s=-M}^M \sum_{t=-M}^M sh(s, t), \\ a_3 = \sum_{s=-M}^M \sum_{t=-M}^M th(s, t), \quad a_4 = \sum_{s=-M}^M \sum_{t=-M}^M s^2 h(s, t), \\ a_5 = \sum_{s=-M}^M \sum_{t=-M}^M t^2 h(s, t), \quad a_6 = \sum_{s=-M}^M \sum_{t=-M}^M sth(s, t) \end{aligned}$$

and f_x, f_y, f_{xx}, f_{yy} and f_{xy} are first- and second-order spatial derivatives in x and y directions respectively. The quality of the approximations (2) and (3) depends on the number of terms in the Taylor-series expansion of the source image $f(x-s, y-t)$. However, $g(x,y)$ in (3) can also be obtained as an inverse Fourier transform of the expression $H(\omega_u, \omega_v)F(\omega_u, \omega_v)$ where $H(\omega_u, \omega_v)$ and $F(\omega_u, \omega_v)$ respectively represent Fourier transforms of the degradation kernel and the source image, $\omega_u = 2\pi u$, $\omega_v = 2\pi v$ and u and v are spatial frequencies in x and y directions. Assuming an image size of $P \times Q$ pixels,

$H(\omega_u, \omega_v)$ is obtained as:

$$\begin{aligned}
H(\omega_u, \omega_v) &= \\
&\sum_{s=-M}^M \sum_{t=-M}^M h(s, t) \exp\left(-j\left(\frac{s\omega_u}{P} + \frac{t\omega_v}{Q}\right)\right) \\
&\cong a_1 - j\omega_u a_2 - j\omega_v a_3 + \\
&\frac{1}{2}\left(\frac{j\omega_u}{P}\right)^2 a_4 + \frac{1}{2}\left(\frac{j\omega_v}{Q}\right)^2 a_5 + \\
&\frac{1}{2}\frac{j\omega_u}{P}\frac{j\omega_v}{Q} a_6,
\end{aligned} \tag{4}$$

which yields:

$$\begin{aligned}
G(\omega_u, \omega_v) &\cong a_1 F(\omega_u, \omega_v) - \\
&a_2 j\omega_u F(\omega_u, \omega_v) - a_3 j\omega_v F(\omega_u, \omega_v) \\
&a_4 \frac{1}{2}\left(\frac{j\omega_u}{P}\right)^2 F(\omega_u, \omega_v) + \\
&a_5 \frac{1}{2}\left(\frac{j\omega_v}{Q}\right)^2 F(\omega_u, \omega_v) + \\
&a_6 \frac{1}{2}\frac{j\omega_u}{P}\frac{j\omega_v}{Q} F(\omega_u, \omega_v).
\end{aligned} \tag{5}$$

Evidently, number of terms in the expansions (4) and (5) depends on the strength of the degradation kernel M , but also on the property of the source image: size of its support $\Omega_x = \Omega_y = \Omega$ in the frequency domain. Thus, degradations with a strength that is small relative to coherence length of the image, i.e. $M \ll (2\pi/\Omega)$, will demand small number of terms in the approximation (3) and vice versa.

When Gabor filters are applied to blurred image, a new set of observed images is obtained as:

$$\begin{aligned}
g_l(x, y) &= a_{l1} f(x, y) - \\
&a_{l2} f_x(x, y) - a_{l3} f_y(x, y) + \\
&a_{l4} f_{xx}(x, y) + a_{l5} f_{yy}(x, y) + a_{l6} f_{xy}(x, y) + \dots
\end{aligned} \tag{6}$$

where

$$\begin{aligned}
a_{l1} &= \sum_{s=-M}^M \sum_{t=-M}^M h_l(s, t), a_{l2} = \sum_{s=-M}^M \sum_{t=-M}^M s h_l(s, t), \\
a_{l3} &= \sum_{s=-M}^M \sum_{t=-M}^M t h_l(s, t), a_{l4} = \sum_{s=-M}^M \sum_{t=-M}^M s^2 h_l(s, t),
\end{aligned}$$

$$a_{l5} = \sum_{s=-M}^M \sum_{t=-M}^M t^2 h_l(s, t), a_{l6} = \sum_{s=-M}^M \sum_{t=-M}^M s t h_l(s, t),$$

and where $h_l(s, t)$ represents convolution of the appropriate l -th Gabor filter with $h(s, t)$. This leads to multi-channel representation:

$$\mathbf{G} = \begin{bmatrix} \mathbf{g}_0^T \\ \mathbf{g}_1^T \\ \dots \\ \mathbf{g}_L^T \end{bmatrix} \cong \begin{bmatrix} a_1 & a_2 & a_3 & a_4 & a_5 & a_6 & \dots \\ a_{11} & a_{12} & a_{13} & a_{14} & a_{15} & a_{16} & \dots \\ \dots & \dots & \dots & \dots & \dots & \dots & \dots \\ a_{L1} & a_{L2} & a_{L3} & a_{L4} & a_{L5} & a_{L6} & \dots \end{bmatrix} \begin{bmatrix} \mathbf{f}^T \\ \mathbf{f}_x^T \\ \mathbf{f}_y^T \\ \mathbf{f}_{xx}^T \\ \mathbf{f}_{yy}^T \\ \mathbf{f}_{xy}^T \\ \dots \end{bmatrix} \tag{7}$$

$$\mathbf{G} \cong \mathbf{A}\mathbf{F}$$

that can be recognized as an LMM to which ICA algorithms can be applied to extract the source image \mathbf{f} . In the simulated and experimental performance evaluation, presented in sections 4 and 5, we have used order of the LMM model set to $L+1=9$, i.e. we have used the real parts of the 2D Gabor filter bank with two spatial frequencies and four spatial orientations ($L=2 \times 4$). Our choice is a reasonable compromise between performance and complexity. For additional information relating to 2D Gabor filter banks, we refer interested readers to [6,7,10,11,12]. We point out that the use of Gabor filters to obtain the LMM (7) is not crucial for the success of the innovations approach to BD that is to be introduced. Some other multi-channel representations, such as wavelet packets, might be used as well. The optimal transform that converts a single sensor to an equivalent of the multi-sensor representation is, at the moment, an open theoretical issue. The lexicographical (vector) representation is assumed in (7) for original image \mathbf{f} and observed images \mathbf{g}_l . In this work we have used a Peano-Hilbert space-filling curve for 2D \rightarrow 1D mapping, due to its property of preserving neighborhood relationships and being amenable to fast implementation [16]. As can be seen no *a priori* information about blurring kernel is assumed so far. There is however a critical condition for the source images \mathbf{f} , \mathbf{f}_x , \mathbf{f}_y , \mathbf{f}_{xx} , \mathbf{f}_{yy} , \mathbf{f}_{xy} etc., to fulfill in order for ICA algorithms to work accurately: in addition to be non-Gaussian, images must be statistically independent as well. The last statement is in general *not true* as already observed in [7] and further elaborated in [10-12].

3 STATISTICAL DEPENDENCE AND INNOVATIONS

We briefly reproduce here results and conditions from [17][12] necessary for the stochastic differentiability of the random source signal \mathbf{f} . Their importance is in establishing conditions for the existence of the Taylor-series expansion, Eq.(2), and the LMM, Eq.(7). First we present two important results that relate (non-)stationarity and linear signal representation. If signal \mathbf{f} is stationary it can be represented by the linear space-invariant generative model:

$$f(p) = \sum_{r=0}^R b(r)\varepsilon(p-r) \quad (8)$$

where $\varepsilon(p)$ is an independent and identically distributed (i.i.d.) driving signal. If signal \mathbf{f} is non-stationary, the linear signal model becomes space-variant:

$$f(p) = \sum_{r=0}^R b(p,r)\varepsilon(p,r) \quad (9)$$

We comment here that \mathbf{f} is a non-stationary signal because its statistics vary locally; i.e., $pdf(f(p_1)) \neq pdf(f(p_2))$. This means that for the typical image the first-order stationarity requirement does not hold [17]. We also comment that image \mathbf{f} is a process with a colored statistics; i.e. it is not an i.i.d. process. This is a consequence of the known phenomenon that neighboring pixels are usually correlated. Consequently its autocorrelation function $\rho_f(\tau)$ differs from the delta function. We are therefore concerned with proving the existence of the Taylor-series expansion, Eq.(2), and LMM, Eq.(7), for a non-stationary and non-i.i.d. process. Although, the conditions required for stochastic differentiability are derived for stationary signals only [17], we can use them with the linear generative model of the non-stationary signal (9). Hence we define derivatives of the non-stationary signal $f(p)$ provided that space variant filter $b(p,r)$ is stationary with respect to the independent variable p :

$$\dot{f}(p) \cong \sum_{r=0}^R \frac{db(p,r)}{dp} \varepsilon(p,r) \quad (10)$$

Thus, Taylor-series expansion (2) and the LMM (7) do exist. However, we can not draw a conclusion regarding statistical independence among \mathbf{f} , \mathbf{f}_x , \mathbf{f}_y , etc., as in the case of a stationary signal, [17][12]. Thus, it is justified to use some of the methods derived to enhance statistical independence between the hidden variables in the LMM (7). In this paper we propose to use innovations

representation of the LMM (7), due to its property of being more non-Gaussian and more statistically independent than original processes. Because these conditions are of essential importance for the success of the ICA algorithms, the unknown basis matrix \mathbf{A} in the LMM (7) will be learned more accurately if ICA algorithms are applied to the innovations representation of \mathbf{G} rather than to \mathbf{G} itself. Once the basis matrix is estimated, we employ its pseudo-inverse to reconstruct the hidden variables in the LMM (7).

Innovations representation has been proposed in [14] as a preprocessing transform in order to increase the accuracy of the instantaneous ICA algorithms. The same approach has also been used later in [18] as the preprocessing transform for linear and post-nonlinear instantaneous ICA problems, when statistically independent source signals have strong temporal autocorrelations. In this later case innovations are implemented by linear preprocessing filter that temporally decorrelates signals which increases their non-Gaussianity. In our approach to BD we use both properties of innovations: increased statistical independence and increased non-Gaussianity, in order to transform the LMM (7) and improve accuracy of the estimation of the basis matrix \mathbf{A} . Innovations representation of the hidden variables contained in \mathbf{F} is

$$\begin{aligned} \tilde{\mathbf{f}}_n(t) &= \mathbf{f}_n(t) - E[\mathbf{f}_n(t) | t, \mathbf{f}_n(t-1), \mathbf{f}_n(t-2), \dots] \\ \mathbf{f}_n &\in \{\mathbf{f}, \mathbf{f}_x, \mathbf{f}_y, \mathbf{f}_{xx}, \mathbf{f}_{yy}, \mathbf{f}_{xy}, \dots\} \end{aligned} \quad (11)$$

where the second term in Eq.(11) represents conditional expectation. If both sides of (11) are multiplied by the unknown basis matrix \mathbf{A} we obtain

$$\tilde{\mathbf{G}} = \mathbf{A}\tilde{\mathbf{F}} \quad (12)$$

Eq.(12) implies that innovations preserve the basis matrix \mathbf{A} . In practice, the expectation is replaced by an autoregressive (AR) model of finite order yielding

$$\begin{aligned} \tilde{\mathbf{g}}_l(t) &= \mathbf{g}_l(t) + b_1\mathbf{g}_l(t-1) + \\ & b_2\mathbf{g}_l(t-2) + \dots + b_K\mathbf{g}_l(t-K) \\ &= \mathbf{g}_l(t) - \hat{\mathbf{g}}_l(t | \mathbf{g}_l(t-1), \dots, \mathbf{g}_l(t-K)). \end{aligned} \quad (13)$$

The coefficients b_k of the AR polynomial are coefficients of the prediction-error filter efficiently estimated by the Levinson algorithm [15]. Thus innovations $\tilde{\mathbf{G}}$ are obtained by applying prediction-error filter on each \mathbf{g}_l

$$\tilde{\mathbf{g}}_l(t) = \sum_{k=0}^K b_k \mathbf{g}_l(t-k), \quad (14)$$

where K represents order of the AR model and $b_0=1$. We identify $L+1$ filters for the LMM model (7) and obtain the prediction-error filter in (14) as an average of the component-wise linear predictors, [18]. Higher order terms in the Taylor series expansion (2), which are caused by strong degradation, may heavily influence quality of the deconvolution result by the proposed algorithm. This is due to the fact that source image and its spatial derivatives act as source signals in the instantaneous LMM (7) and they are statistically dependent. At the moment it is an open issue to what extent linear preprocessing transforms, such as innovations proposed here or wavelet packets proposed in [12] can enhance statistical independence among this special class of hidden variables i.e. source image and its higher-order spatial derivatives? Therefore, we make an assertion that efficiency of the proposed approach to BD might be limited in cases of strong degradations that consequently induce presence of higher-order spatial derivatives of the source image in the LMM (7).

4 SIMULATION RESULTS ON DE-FOCUSED IMAGE

Table 1 and Figure 1 show the results of the comparative performance analysis between derived algorithm, wavelet-packets (WP) based algorithm [12]

Table 1. Rows: SIR performance, Eq. (15), for: blurred image; image restored by innovations-based algorithm; image restored by WP algorithm [12]; image restored by BRL algorithm after 10 iterations with $R=3$; image restored by BRL algorithm after 10 iterations with $R=5$. Columns: Type of algorithm; size of degradation kernel $R=3$ pixels; size of degradation kernel $R=5$ pixels.

	Blurred image	Innovations	WP [12]	BRL, R=3	BRL, R=5
SIR [dB], R=3 pixels	17.07	21.46	17.80	22.61	15.81
SIR [dB], R=5 pixels	13.68	14.71	13.20	14.42	17.93

Several conclusions can be drawn from these results. The performance of the proposed image restoration algorithm as well as the WP algorithm decreases as strength of degradation process is increased. The same conclusion holds for the BRL algorithm. However, performance of the BRL algorithm decreases rapidly when the size of the degradation kernel is not estimated correctly. This is a demonstration of the known fact that BD algorithms are in general very sensitive to either over- or underestimation of the size of degradation kernel [2]. In addition to that, if the size of degradation kernel is

and blind Richardson-Lucy (BRL) algorithm [19], implemented by a MATLAB[®] command `deconvblind`. We have simulated de-focus blur by convolution of the image with a circular kernel with radius $R=3$ and $R=5$ pixels. The size of the original *bacteria-AT3* image, taken from the MATLAB[®] image processing toolbox is 480×640 pixels. The JADE-ICA algorithm [20] was applied to innovations representation $\tilde{\mathbf{G}}$ to learn the basis matrix \mathbf{A} . In the implementation of the innovations, the order of the prediction-error filter (14) was set to $K=10$ (the choice is not critical). In order to quantify performance of the image restoration algorithms we have calculated signal-to-interference ratio (SIR) in dB according to:

$$SIR_{dB} = -10 \log_{10} \left(\frac{\sum_{x=1}^P \sum_{y=1}^Q (f(x,y) - \hat{f}(x,y))^2}{\sum_{x=1}^P \sum_{y=1}^Q f(x,y)^2} \right) \quad (15)$$

where $f(x,y)$ and $\hat{f}(x,y)$ denote reference and restored image respectively. When SIR was calculated for blurred image, $\hat{f}(x,y)$ in (15) had to be replaced with $g(x,y)$. The SIR performance is summarized in Table 1.

not known, the BRL algorithm has to be run several times before the best result can be selected. There are no such problems with the proposed method. Selected results for this simulated scenario are shown in Figure 1. We would like to comment on the shape of the magnitude frequency response of the prediction-error filter used in (14) to implement innovations representation. The shape of the response reveals the known empirical fact that statistical dependence is concentrated in the low-frequency part of the spectrum, which is typical for the real-world images [13].

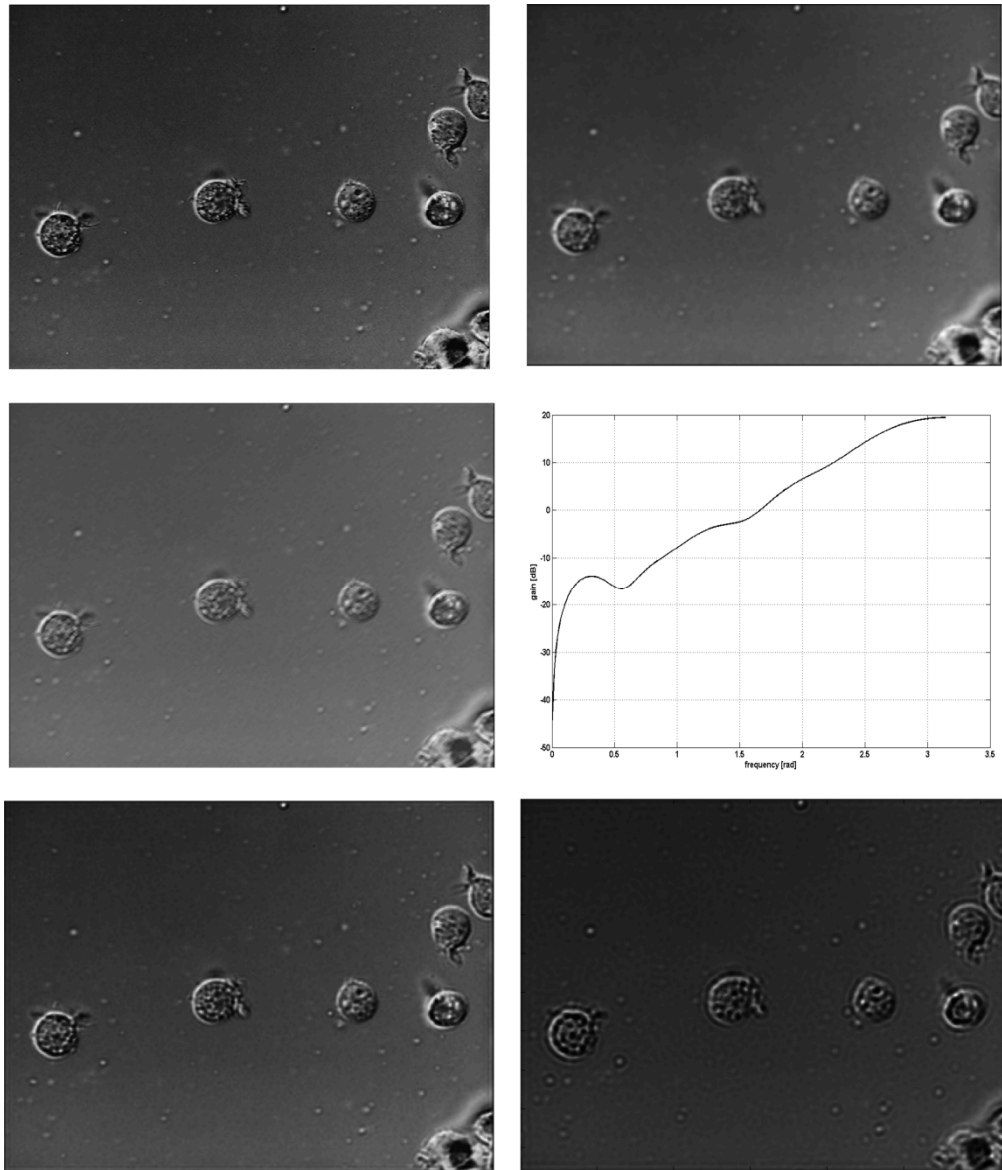


Fig. 1. Top left: original bacteria-AT3 image; top right: defocused image with radius of circular blurring kernel $R=3$ pixels; middle left: image restored by the proposed algorithm; middle right: magnitude frequency response of the prediction-error filter; bottom left: image restored by the BRL algorithm after 10 iterations and assumed radius of the blurring kernel $R=3$ pixels; bottom right: similar as left but with the $R=5$ pixels.

5 EXPERIMENTAL RESULTS ON DEFOCUSED IMAGE

Figure 2 shows de-focused image obtained by digital camera in manually de-focused mode, the image restored by the innovations approach, the magnitude frequency response of the learned prediction-error filter used to implement the innovations transform and the image

restored by the BRL algorithm. The order of the prediction-error filter, Eq.(14), used to implement innovations transform was set to $K=10$. The JADE algorithm [20] was applied to the innovations of the LMM to learn the basis matrix. Similarly to the case with the simulated de-focusing blur, shape of the magnitude frequency response of the prediction-error filter obeys high-pass filtering behavior. Consequently, we have achieved good agreement between simulation and

experiment. We want to stress again that shape of the frequency response is optimally adapted to the specific experimental image. The BRL result was obtained after 10 iterations with the radius of the circular blurring kernel equal to $R=3$ pixels. We want to point out that the BRL algorithm had to be run several times for different values

of the size of the blurring kernel R . Then the image with the best quality had to be chosen. There are no such problems with the innovations-based algorithm. Hence we expect it can be useful in many real-world applications [21].

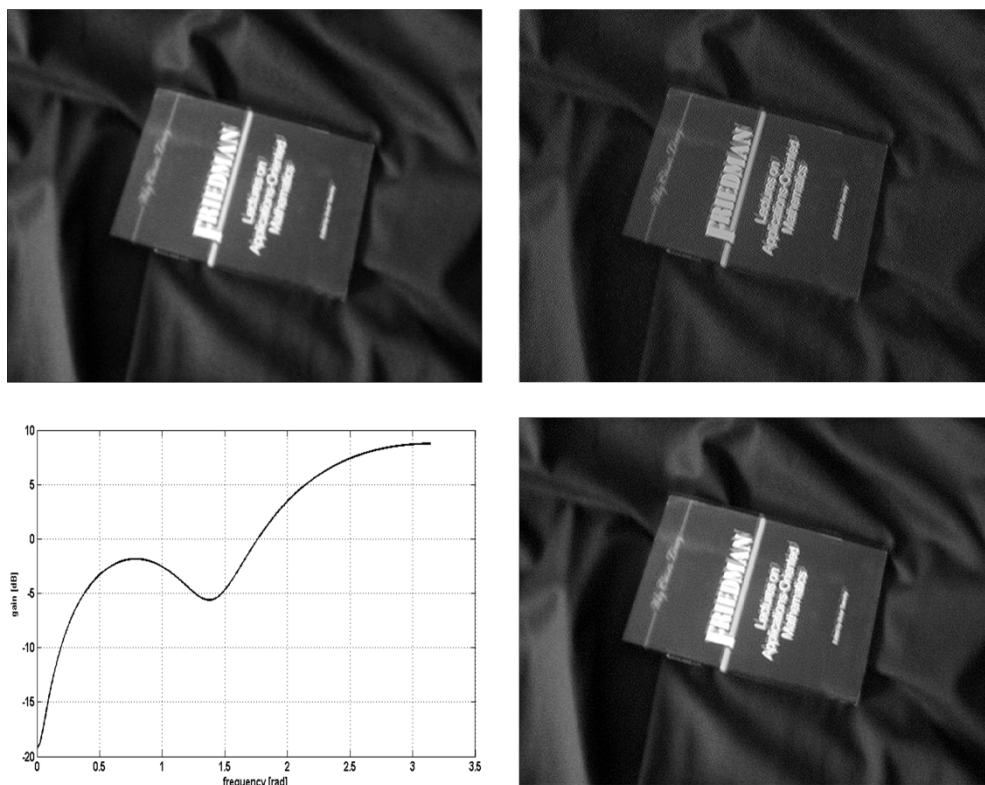


Fig. 2. Top left: de-focused experimental image; top right: image restored by the proposed algorithm; bottom left: magnitude frequency response of estimated prediction-error filter, bottom right: the best result obtained by BRL algorithm with $R=3$ pixels.

6 CONCLUSION

An approach to single frame multi-channel blind image deconvolution has been introduced requiring no information about the size and origin of the blurring or convolution kernel. The approach is characterized by converting blind deconvolution problem into an instantaneous blind source separation problem of statistically dependent sources, where hidden variables are source image and its higher-order spatial derivatives. In relation to the competing algorithms introduced recently, we have used innovations representation of the resulting linear mixture model in order to estimate the unknown basis matrix. We have demonstrated consistent performance by the introduced algorithm on simulated

and experimental de-focused image. The shape of the magnitude frequency response of the estimated prediction-error filter revealed known empirical fact that statistical dependence is concentrated in the low-frequency part of the spectrum. Quantitative performance expressed in term of the signal-to-interference ratio confirmed that the proposed algorithm successfully competes with the state-of-the-art blind image deconvolution algorithms, such as blind Richardson-Lucy algorithm, requesting no information about the size and origin of degradation kernel. The open questions that ought to be answered are: optimality of the transform used to convert single-sensor to multi-sensor problem and optimality of the transform used to enhance statistical independence among the special class of hidden variables that consists of the source image and its higher-order

spatial derivatives.

ACKNOWLEDGMENTS

The authors gratefully acknowledge help of Professor Andrzej Cichocki for providing code that calculates the SIR performance measure. Part of this work was supported through grant 098-0982903-2558 funded by the Ministry of Science, Education and Sport, Republic of Croatia.

REFERENCES

- [1] M.R. Banham, A.K. Katsaggelos, Digital Image Restoration, IEEE Signal Processing Magazine 14 (1997) 24-41.
- [2] D. Kundur, D. Hatzinakos, Blind Image Deconvolution, IEEE Signal Processing Magazine 13 (1996) 43-64.
- [3] K. E. Jang, J. C. Ye, Single channel blind image deconvolution from radially symmetric blur kernels, Optics Express 15 (2007) 3791-3803.
- [4] A. Hyvärinen, J. Karhunen, E. Oja, Independent Component Analysis, John Wiley & Sons, Inc, New York, 2001.
- [5] I. Kopriva, Q. Du, H. Szu, W. Wasyliwskyj, Independent Component Analysis Approach to Image Sharpening in the Presence of Atmospheric Turbulence, Optics Communications 233 (2004) 7-14.
- [5a] Q. Du, I. Kopriva, Dependent Component Analysis for Blind Restoration of Images Degraded by Turbulent Atmosphere, Neurocomputing 72 (2009), 10-12; 2682-2692
- [6] S. Umeyama, Blind Deconvolution of Blurred Images by Use of ICA, Electronics Communication in Japan, Part 3 84 (2001), 1-9.
- [7] J. G. Daugman, Complete Discrete 2-D Gabor Transforms by Neural Networks for Image Analysis and Compression, IEEE Tr. on Acoustics, Speech and Signal. Processing 36 (1988) 1169-1179.
- [8] M. Numata, and N. Hamada, Image Restoration of Multichannel Blurred Images by Independent Component Analysis, in Proceedings of 2004 RISP International Workshop on Nonlinear Circuit and Signal Processing (NCSP'04, 2004), pp.197-200.
- [9] P. O. Hoyer, Non-negative matrix factorization with sparseness constraints, Journal of Machine Learning Research 5 (2004) 1457-1469.
- [10] I. Kopriva, Single Frame Multichannel Blind Deconvolution by Non-negative Matrix Factorization with Sparseness Constraint, Optics Letters 30 (2005) 3135-3137.
- [11] I. Kopriva, D.J. Garrood, V. Borjanović, Single Frame Blind Image Deconvolution by Non-negative Sparse Matrix Factorization, Optics Communications 266 (2006) 456-464.
- [12] I. Kopriva, Approach to Blind Image Deconvolution by Multiscale Subband Decomposition and Independent Component Analysis, Journal Optical Society of America A 24 (2007) 973-983.
- [13] A. Cichocki, P. Georgiev, 'Blind source separation algorithms with matrix constraints, IEICE Transactions on Fundamentals of Electronics, Computer and Computer Science E86-A (2003) 522-531.
- [14] A. Hyvärinen, Independent component analysis for time-dependent stochastic processes, in: Proceedings of the International Conference on Artificial Neural Networks (ICANN'98, 1998), pp. 541-546.
- [15] S. J. Orfanidis, Optimum Signal Processing – An Introduction, 2nd ed., MacMillan Publishing Comp., New York, 1988.
- [16] W. M. Lam, J. M. Shapiro, A Class of Fast Algorithms for the Peano-Hilbert Space Filling Curve, in: Proceedings of the IEEE International Conference Image Processing, Institute of Electrical and Electronics Engineers, New York, 1994, pp. 638-641.
- [17] M. B. Priestley, Spectral Analysis and Time Series, Academic Press, 1981.
- [18] J. Karvanen, T. Tanaka, Temporal Decorrelation as Preprocessing for Linear and Post-nonlinear ICA, Lecture Notes in Computer Science 3195 (2004) 774-781.
- [19] D. A. Fish, A.M. Brinicombe, E.R. Pike and J.G. Walker, Blind deconvolution by means of the Richardson-Lucy algorithm, Journal Optical Society of America 12 (1995) 58-65.
- [20] J. F. Cardoso, A. Soulomniac, Blind beamforming for non-Gaussian signals, Proceedings. IEE F 140 (1993) 362-370.
- [21] G. K. Klančar, M. Brezak, D. Matko, I. Petrović, Mobile Robots Tracking Using Computer Vision, Automatika 46 (2006) 155-163.